Laser and Particle Beams (2015), *33*, 655–666.

doi:10.1017/S0263034615000671

Irradiation asymmetry effects on the direct drive targets compression for the megajoule laser facility

N.N. DEMCHENKO,[1] I.YA. DOSKOCH,[1] S.YU. GUS'KOV,[1] P.A. KUCHUGOV,[1,2] V.B. ROZANOV,[1] R.V. STEPANOV,[1] G.A. VERGUNOVA,[1] R.A. YAKHIN,[1] AND N.V. ZMITRENKO[2]

[1]P.N. Lebedev Physical Institute of the Russian Academy of Sciences, Moscow, Russia
[2]Keldysh Institute of Applied Mathematics of the Russian Academy of Sciences, Moscow, Russia

(Received 9 June 2015; Accepted 12 June 2015)

Abstract

In the previous works (Rozanov *et al*., 2013; 2015) we have performed one-dimensional (1D) numerical simulations of the target compression and burning at the absorbed energy of ~1.5 MJ. As a result, the target was chosen to have a low initial aspect ratio in order to be less sensitive to the influence of such parameters as laser pulse duration, total laser energy, and equations of state model. The simulation results demonstrated a higher probability of ignition and effective burning of such a system. In the present work we discuss the impact of irradiation asymmetry on this baseline target implosion. The details of the 1D compression and a possible influence of 2D and 3D effects due to the hydrodynamic instability and mixing have been described. In accordance with the 2D calculations the target is still ignited, however, the symmetry analysis of 3D ones gives reasons to further reduce the efficiency of conversion of kinetic energy into potential energy.

Keywords: Irradiation asymmetry; Laser driven fusion; Mathematical modeling; Target stability

1. INTRODUCTION

Laser-driven fusion is to one of the most urgent and practically important problems of modern physics, since its aim is to create an inexhaustible source of energy, and it is currently based on the pilot program carried out in the Lawrence Livermore National Laboratory (LLNL, USA) on high-power laser facility called the National Ignition Facility (Miller *et al*., 2004; Moses *et al*., 2009; Landen, 2014). The laser parameters (up to 1.9 MJ, 192 laser beams), according to current projections, allow ignition of a thermonuclear target followed by the release of a large amount of energy at the burning stage. To date, target ignition has not been achieved in experiments and the reasons for failure are not fully established, which makes the problem of laser fusion even more physically meaningful.

Discussing the problem of laser fusion, one should keep in mind the working OMEGA facility (USA, 30 kJ, 3ω, 60 beams) (Boehly *et al*., 1997), Laser Mégajoule (LMJ) facility (France, 1.4 MJ, 3ω, 176 beams, completion of construction is planned for 2015–2016) (Besnard, 2008; Ebrardt & Chaput, 2008; Miquel, 2014), and the projected facility in Russia (2 MJ, 2ω, 192 beams) (Garanin *et al*., 2012). These data indicate the scale and scope of current research programs. The Direct- and indirect-drive targets are considered. Meanwhile, experiments with megajoule pulses are performed only with the indirect-drive targets, when the energy of a laser pulse is converted into a soft X-ray radiation, which vaporizes the ablator and causes compression of the target. The direct-drive targets for laser megajoule pulses are considered as conceptual schemes.

In these schemes the approach based on achieving maximum values of parameters of the compression and burning (Edwards *et al*., 2011; Brandon *et al*., 2013; Clark *et al*., 2013) is still used. However, the practice and the results of the National Ignition Campaign (Edwards *et al*., 2013) make a different approach relevant which is to find such target schemes and organization of processes that the resulting target ignition should be less sensitive to possible incomplete knowledge of plasma properties and to probable deviations of the compression conditions from those that are assumed in the mathematical modeling of the experiments. Realization of low-sensitivity regimes of target ignition can be achieved at the expense of refusal to fulfill the maximum values of the neutron yield.

It is now believed that the main obstacle to the achievement of self-sustaining thermonuclear burning is the development

Address correspondence and reprint requests to: Pavel A. Kuchugov, Russian Federation, Miusskaya Sq. 4, 125047 Moscow, Russia. E-mail: pkuchugov@gmail.com.

of various kinds of instabilities. Many different sources of these instabilities, as well as the parameters of laser fusion problems exist, and from our point of view the capability to analyze their joint impact on the dynamics of target compression is very limited due to its complexity. Eliminating sources of instabilities can be achieved by improving the technological processes involved in preparation of the capsule with thermonuclear fuel and the laser-optical system, which is a matter of time (perhaps long enough), or by leveling of their impact (i.e., searching for terms and conditions that are less sensitive to the subject negative effect) due to special designs of thermonuclear targets and laser systems (Brandon *et al.*, 2014; Rozanov *et al.*, 2015). For example, in (Rozanov *et al.*, 2015), the optimization of target design based on one-dimensional (1D) calculations using the program DIANA (Zmitrenko *et al.*, 1983) program was carried out for the planned Russian laser facility, the basic parameters of which were presented in (Garanin *et al.*, 2012; Rozanov *et al.*, 2013), and its stability against deviations from the basic values of various parameters such as the duration of the laser pulse, the total energy of the laser pulse, the model of equations of state (EOS), and the aspect ratio of the deuterium tritium (DT)-layer was investigated.

In this paper, which is a logical continuation of (Rozanov *et al.*, 2015), the information obtained in 1D calculations, is systematized taking into account the change of optimization strategy, as mentioned above. Based on these data 2 and 3D calculations were formulated and carried out.

Here we give the parameters of baseline target, produced on the basis of the above optimization. The composition and sizes of the shells are illustrated in Figure 1. The total target mass is 2182.9 μg, mass of DT-gas, 12 μg ($\rho = 10^{-3}$ g/cc), mass of DT-ice, 1054 μg ($\rho = 0.253$ g/cc), and mass of ablator (CH), 1117 μg ($\rho = 1.05$ g/cc). To determine the thermodynamic properties of substances the EOS in the Thomas–Fermi model was used in the final version of the 1D calculation, which resulted in the following values of the main parameters of the implosion: thermonuclear gain G – 17.95, maximal hydro-efficiency η_{max} – 6.54%, which corresponds to a maximum implosion velocity of about 411 km/s, evaporated mass – 1035 μg (93% of ablator mass); energy losses on bulk emission to the end of the implosion (i.e., taking into account the combustion) are 0.402 MJ or 27% of total absorbed laser energy, or 1.5% of the released fusion energy, or 8.8% of fusion energy absorbed in the target. The maximum achievable average density of DT-ice is 116.4 g/cc at time 10.99 ns. At this point parameter $\alpha = p/p_F$ is approximately 5–6 in the cold part of the DT-fuel. The dynamics of the target compression is well illustrated by the *R-t* diagram of DT-ice layer boundaries shown in Figure 2.

When discussing issues related to the development of hydrodynamic instabilities, it is interesting to analyze the effect of the DT-layer aspect ratio computed as $A_{DT} = R^{ex}_{DT}/\left(R^{ex}_{DT} - R^{in}_{DT}\right)$ on the efficiency of target burning. Using Figure 2, one can calculate that at the initial time moment the value of A_{DT} for the baseline target is 10.4 (denoted by A^0_{DT}). At constant pulse and target mass (both fuel and ablator) we obtain the following dependence of the gain on the aspect of the DT-layer (shown in Fig. 3). By increasing the aspect ratio from the value A^0_{DT} a decline in thermonuclear gain by reducing the surface density ρR (Dolan, 1981; Lindl, 1995) is observed. In the opposite case, G increases to a threshold value determined mainly by the reduction of the ion temperature below the radiation limit, and then falls sharply. Taking into account the fact that the low-aspect-ratio targets are more stable to perturbations during implosion (Volosevich *et al.*, 1995; Brandon *et al.*, 2013, 2014), the range of A_{DT} from 6.5 to 8 seems promising. However, the use of such targets in the case of possible variations in the various parameters (e.g., the absorbed energy) increases the risk of crossing the threshold and shifting into the range of inefficient burning, or its absence. Thus, the base target is selected from the conditions that are far enough from those that ensure the maximum neutron yield ($G \approx 45$).

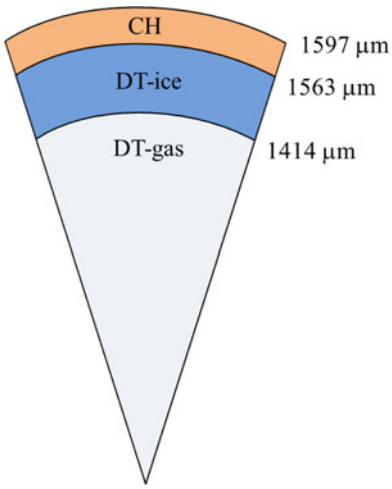

Fig. 1. Composition and sizes of the shells of the baseline target.

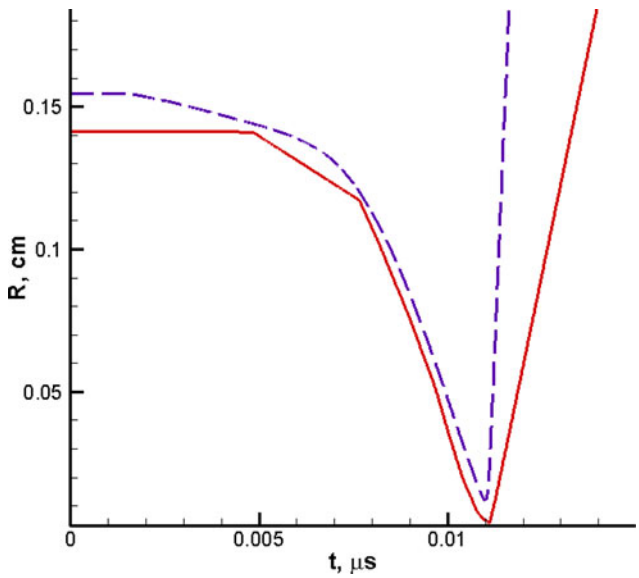

Fig. 2. *R-t* diagrams of DT-ice boundaries for the baseline target.

https://doi.org/10.1017/S0263034615000671 Published online by Cambridge University Press

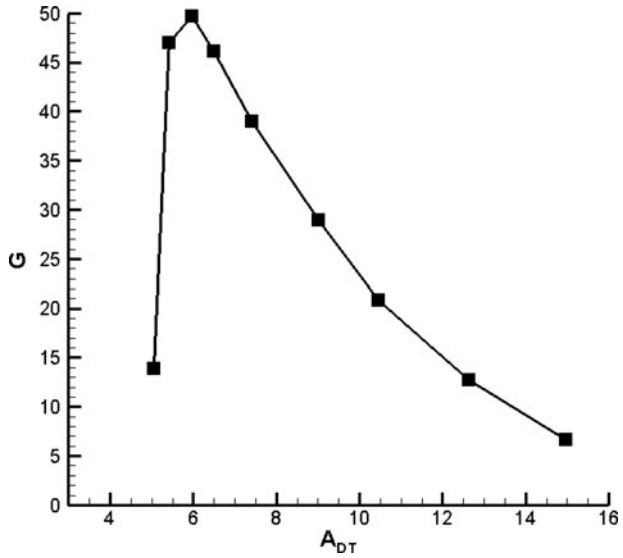

Fig. 3. Dependence of the thermonuclear gain G on the value of the aspect ratio A_{DT}.

In addition to variations in the parameters of the laser pulse, and possible deviations of the matter state from that expected, which are mentioned above, another source causing the development of the instabilities is the inhomogeneity of the target irradiation. This work is devoted to the study of the influence of irradiation inhomogeneity on the efficiency of target compression and thermonuclear burning taking into account the development of 2 and 3D flows.

2. SYMMETRY OF IRRADIATION AND ENERGY DEPOSITION

Let us recall the assumed conditions of irradiation (Garanin *et al.*, 2012; Rozanov *et al.*, 2013, 2015). As the working wavelength of planned laser facility the wavelength of second harmonic of Nd-laser is chosen which has the value of 0.530 μm. The total energy of the laser pulse is 2 MJ. The irradiation occurs along the sides of the cube, on each of them eight clusters consisting of four beams are located

Table 1. *Dependencies of the proportion of absorption and the degree of absorbtion homogeneity on the characteristic radius of the beam for different values of n in (1), and different conductivity models*

a/R_0	$n = 2, f = 0.06$		$n = 4, f = 0.06$		$n = 2$, Spitzer	
	δ_a	η_E	δ_a	η_E	δ_a	η_E
0.5	0.755	0.9396	0.779	0.9081	0.956	0.8703
0.6	0.722	0.9593	0.758	0.9007	0.928	0.9219
0.7	0.686	0.9566	0.734	0.9108	0.892	0.9566
0.8	0.648	0.9525	0.707	0.9246	0.849	0.9716
0.9	0.609	0.9554	0.676	0.9416	0.802	0.9791
1.0	0.570	0.9663	0.642	0.9661	0.754	0.9661
1.1	0.533	0.9678	0.608	0.9680	0.705	0.9711
1.2	0.498	0.9725	0.574	0.9671	0.657	0.9705
1.3	0.465	0.9741	0.540	0.9697	0.612	0.9626

(see Fig. 4a). The radiation intensity distribution in the plane passing through the center of the target and perpendicular to the optical axis of the beam has the form

$$I(r) = I_0 \exp\left[-\left(\frac{r}{a}\right)^n\right], \quad (1)$$

where r is the distance from the optical axis, a, characteristic radius of the beam, and I_0, intensity on the optical axis. Calculation of the laser energy absorption was conducted using numerical code RAPID (Afanas'ev *et al.*, 1982). Different values of n in Eq. (1) as well as various models of thermal conductivity (Spitzer model and one using the flux limiting parameter $f = 0.06$) were considered while performing the simulations. Dependencies of the quantities characterizing the absorption of laser energy on specified parameters are shown in Table 1. Here δ_a is the proportion of absorption, $\eta_E = E_t^{min}/E_t^{max}$, the degree of absorption homogeneity, where E_t is absorbed energy, R_0, radius of the target at initial time moment ($R_0 = 1595$ μm in this work). Note that η_E increases with increasing radius of the beam. Using a model of the limited thermal conductivity for $n = 2$ and $n = 4$ in the case of $a/R_0 \geq 1$ η_E takes almost equal values, and using

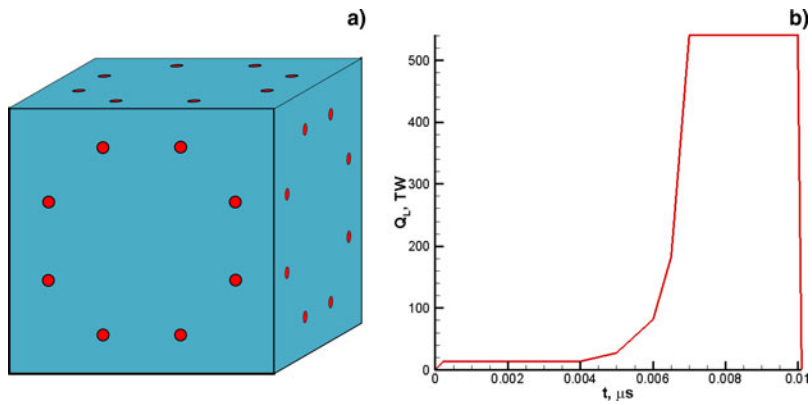

Fig. 4. (a) Symmetry of the irradiation of the thermonuclear target; (b) time dependence of the incident laser flux power Q_L.

https://doi.org/10.1017/S0263034615000671 Published online by Cambridge University Press

the model of Spitzer conductivity, since $a/R_0 = 0.8$ the value η_E is changing slightly. In further calculations we use Gaussian beam ($n = 2$) and the model with a limited thermal conductivity ($f = 0.06$) as the most adequately describing the experimental results of the interaction of nanosecond laser pulse with plasma (Volosevich *et al.*, 1978; Basov *et al.*, 1988; Dolgoleva, 2013).

For the considered multi-beam system and parameters $n = 2$, $a/R_0 = 1$, $f = 0.06$ in Figure 5 the angle distribution of absorbed energy during the laser pulse is shown. On this map one can select the area limited by angles' ranges $0° \le \varphi \le 45°$ (azimuthal angle) and $0° \le \theta \le 90°$ (polar angle) which with the help of elementary transformations can be translated to the rest of the o sphere surface. Due to the need for further detailed 1D numerical simulation, we need to allocate some of the most interesting points in the elementary region, namely the points sufficiently different from each other in terms of irradiation conditions. In this study, 18 points were chosen that are marked with white circles in Figure 5. Let us give to them dependencies of function of the angular distribution of the absorbed flux W on time (see Figs. 6a–6c). Function W is normalized so that its average value over the solid angle 4π is 1. Figure 6d shows the dependence of the efficiency of absorption of laser energy δ_{abs} from time. The dependence of the absorbed laser flux Q_a defined by the expression $Q_a(t, \varphi, \theta) = Q_L(t)W(t, \varphi, \theta)$. This value is used for further 1D numerical calculation. Note that due to the symmetry of the cube according to the values of $W(t)$ for $\theta = 0°$ and $\theta = 90°$ for $\varphi = 0°$ are the same. Dependencies also coincide for all φ at $\theta = 0°$.

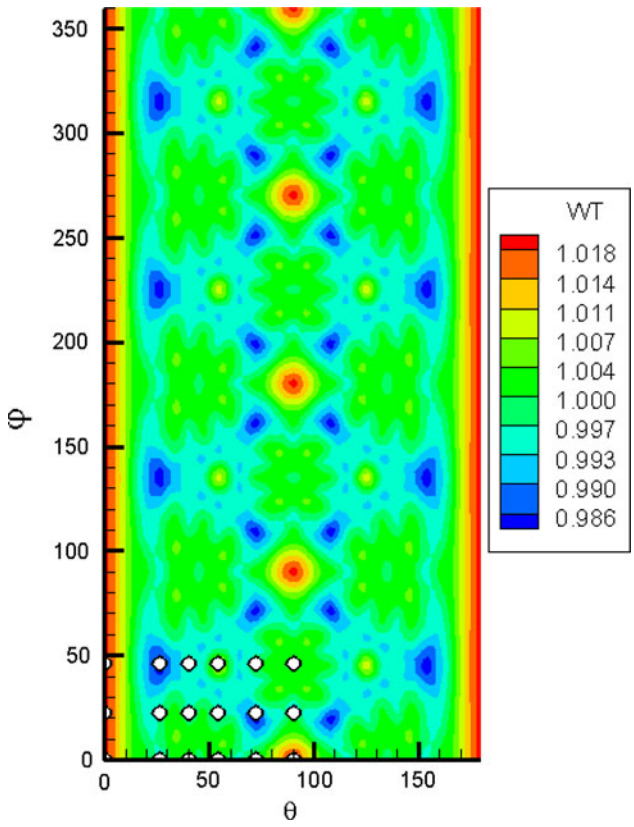

Fig. 5. Angular distribution of the absorbed energy on account of inverse Bremsstrahlung during the laser pulse ($a/R_0 = 1$, $n = 2$).

Another important factor identified by the study of the efficiency of absorption of laser irradiation is the displacement of the surface of characteristic density at which the energy is deposited from the target center due to refraction. In the following 1D calculations this fact was taken into account due to the adjustment of the wavelength of the incident laser irradiation, namely, reducing the effective value of the critical density ($\rho_{cr} \sim \lambda^{-2}$).

3. DETAILED 1D SPHERICALLY SYMMETRIC CALCULATIONS AND CONDITIONS FOR INSTABILITIES DEVELOPMENT

For the 18 points on the sphere chosen in the previous section, characterized by the angles θ = 0, 26, 40, 54, 72, and 90, and φ = 0, 22, and 46, 1D calculations of baseline target compression and burning with the parameters that are discussed in Section 1 were carried out using the DIANA program (Zmitrenko *et al.*, 1983). For simulations of target compression this Lagrangian numerical code uses one-fluid two-temperature model and also takes into account electron and ion heat transfer, the exchange of energy between ion and electron components, local energy deposition from thermonuclear reactions, burning out of DT-fuel, volume energy losses due to bulk emission, and incident laser flux absorption due to inverse Bremsstrahlung mechanism and resonant one in the vicinity of critical density. The main difference between performed series of calculations in comparison with the previous one (Rozanov *et al.*, 2015) is that the absorption of the laser radiation is δ-shaped manner on the surface of the target, where the density is about 76% of the critical one which corresponds to the second harmonic Nd-laser radiation. The following Table 2 shows the basic quantities characterizing the compression and burning of the target for each of the calculations. In all calculations, taking into account the variations in the absorption coefficient depending on the position of the point on the sphere, the value of the target thermonuclear gain G varied in the range of 8–14, and the absorbed energy E_t in the range 1.47–1.53 MJ. Below in Figure 7 dependency of the gain on the absorbed energy (i.e., irradiation conditions) is presented which characterizes the spreading values of G in the conducted series of 1D calculations.

Let us analyze the scale of the differences between the calculations due to the inhomogeneity of irradiation of the target using the radius of the outer surface of DT-ice, taken at the time moment $t = 10$ ns. The values between the points on the sphere, which correspond to 1D calculations are determined by interpolation using cubic splines (Kalitkin, 1978). The resulting distribution of radius values is shown in Figure 8. It is seen that the spread of these values is calculated by the formula $\delta_\psi = 2(\psi_{max} - \psi_{min})/(\psi_{max} + \psi_{min})$, where $\psi \equiv R_{DT/CH}$ is 2%, which indicates a relatively weak

https://doi.org/10.1017/S0263034615000671 Published online by Cambridge University Press

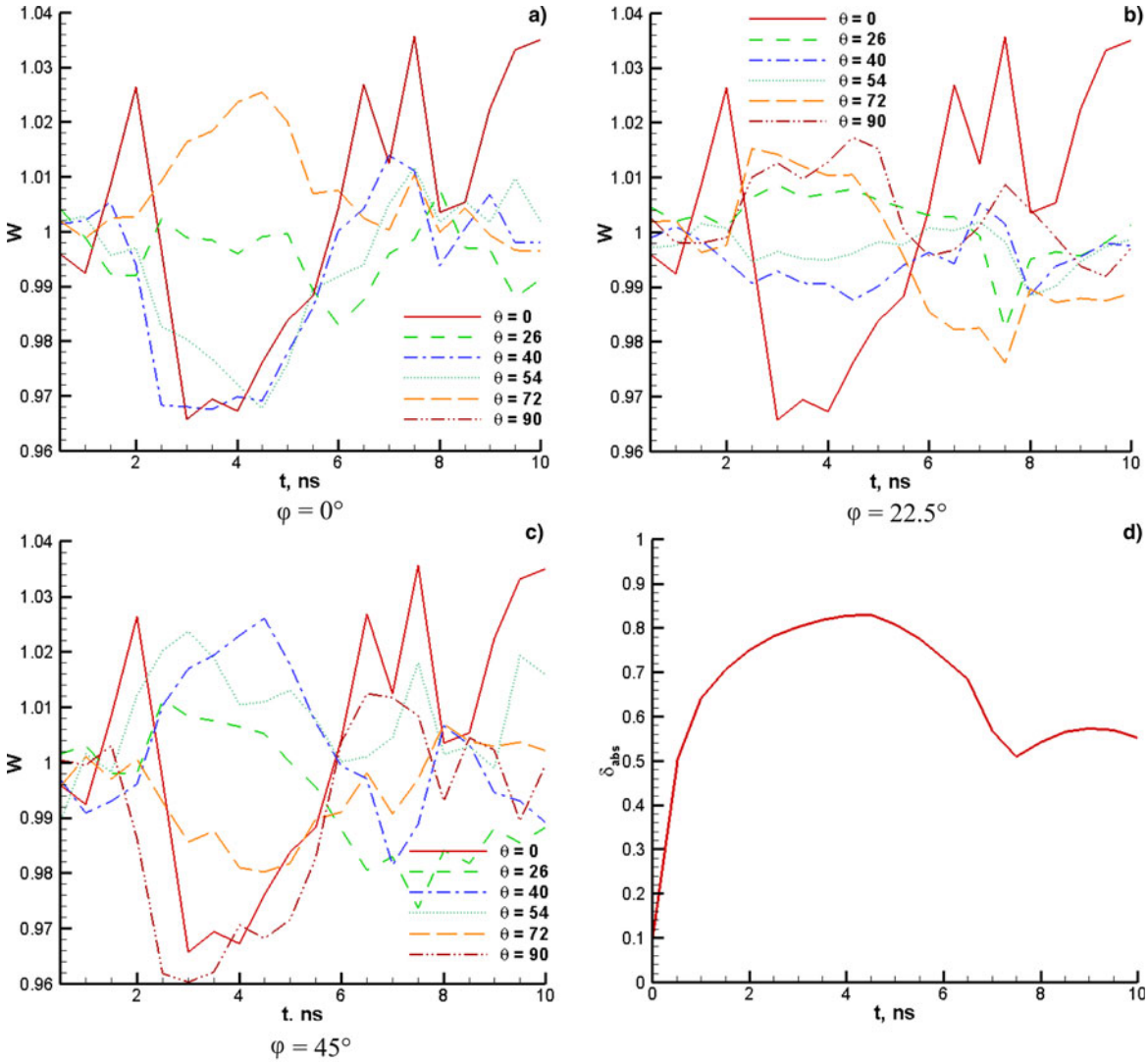

Fig. 6. (a)–(c) Time dependence of the function of the angular distribution of the absorbed flux; (d) time dependence of the absorption efficiency.

influence of irradiation asymmetry on the target compression dynamics. Note that, as expected, the resulting distribution of radii is correlated with absorbed energy map as shown in Figure 3: Points with a smaller radius correspond to large values of absorbed energy.

Such an interpolation procedure may be performed for other values. For example, the dispersion values of the radial velocity at the surface of the DT-ice/ablator are 6 km/s ($\delta_V \approx 1.7\%$), density, 0.61 g/cc ($\delta_\rho \approx 4\%$), pressure, 15.1 Mbar ($\delta_p \approx 8\%$). The data in Table 2 show some impact of the considered irradiation conditions on the parameters characterizing a 1D spherical compression and burning of the target, but they do not lead to the disruption of ignition.

Let us analyze the conditions for the development of instabilities in the calculation example # 1 in Table 2. We shall follow up the values of density, pressure, velocity, temperature, acceleration, and adiabatic curve at a point inside DT-layer, namely, at a distance of 1443 μm from the center at the initial time moment. These dependences are shown in Figure 9. Areas of positive acceleration in Figure 9b correspond to deceleration of inward motion of DT-layer and cause instabilities development. For these conditions of laser energy absorption the collapse of the target occurs approximately at time $t = 11.25$ ns, followed by the explosion, which is not discussed in this work.

With the data presented in Figure 9, one can say that at the moment of maximum compression ($t = 11.25$ ns) radius of the inner surface of DT-layer is $R_{\min}^{\text{inner}} \approx 50$ μm, and the outer one is approximately $R_{\min}^{\text{outer}} \approx 130$ μm. Classic increment of Rayleigh–Taylor instability is given by the formula $\gamma_0^2 = kAg_0$, where A, Atwood number, k, wave vector and can be calculated by referring to Figure 9b. The average value of the deceleration is found to be $g_0 \equiv \langle a \rangle 5.10^5$ cm/μs^2, the duration of which is about $\Delta t \approx 0.1$ ns. According to the data of the irradiation inhomogeneity one can estimate the most significant for instability development wavenumber of

https://doi.org/10.1017/S0263034615000671 Published online by Cambridge University Press

Table 2. *Integral characteristics of 1D numerical simulations corresponding to different pairs of angles (θ, φ). Here η_{max} (%) is the maximal hydro-efficiency, $(\rho R)_{max}$, the maximal optical thickness of the region occupied by DT,* G, *the thermonuclear gain,* E_r, *the radiation energy losses,* t_C, *the collapse time,* R_{HS}, *the radius of the hot-spot defined by ion temperature 7 keV,* V_{max}, *the maximal velocity of implosion*

##	θ	φ	t_C, *ns*	η_{max}, %	$(\rho R)_{max}$, g/cm^2	*G*	R_{HS}, μ*m*	V_{max}, km/s	E_r, MJ
1	0	0	11.246	5.8595	0.8394	13.508	79.208	389.2	0.39381
2	26	0	11.282	5.8918	0.8067	10.252	77.260	383.7	0.34284
3	40	0	11.274	5.8887	0.8138	11.094	78.244	384.7	0.35662
4	54	0	11.273	5.8910	0.8188	11.498	77.891	385.0	0.36274
5	72	0	11.262	5.8636	0.8051	11.094	77.947	384.0	0.35704
6≡1	90	0	These are the same as in the calculation #1						
7≡1	0	22	These are the same as in the calculation #1						
8	26	22	11.280	5.8732	0.8042	10.039	77.537	382.7	0.33918
9	40	22	11.280	5.8889	0.8074	10.391	77.777	383.7	0.34490
10	54	22	11.281	5.8856	0.8072	10.445	77.663	383.5	0.34597
11	72	22	11.296	5.8994	0.7975	9.0295	76.366	381.7	0.32002
12	90	22	11.268	5.8734	0.8117	11.268	78.260	383.8	0.35250
13≡1	0	46	These are the same as in the calculation #1						
14	26	46	11.305	5.9019	0.7933	8.5764	76.083	381.3	0.31095
15	40	46	11.280	5.8822	0.8145	10.941	77.369	382.8	0.35402
16	54	46	11.256	5.8534	0.8198	11.696	78.963	384.7	0.36688
17	72	46	11.277	5.8990	0.8233	11.902	77.901	384.6	0.36834
18	90	46	11.277	5.8947	0.8132	11.044	77.899	384.6	0.35605

spherical harmonic as $l \approx 8$–10. Assuming for estimates $A \approx 1$ and $k \approx l/R_{\min}^{\text{outer}}$ we get $\gamma_0 \approx 20\ \text{ns}^{-1}$ and growth factor $\Gamma = \gamma_0 \Delta t \approx 2$. Note that this is a very modest value. Thus, the initial perturbation of the shell with amplitude equal $\Delta R/2 \approx 5$ μm (see Fig. 8) grows approximately 7.4 times, reaching a value of about 40 μm when the DT-ice shell thickness is about 80 μm (see Figure 9e) at the time moment $t = 11.25$ ns. This means that there is strong mixing of ablator with the fuel.

Note that the estimations of the instability development were performed using linear theory which is not quite true. Namely, the characteristic wavelength is $\lambda_c \approx R_{\min}/l \approx$ 10 μm that is of the same order as the initial amplitude. As it is known, the development of hydrodynamic instability

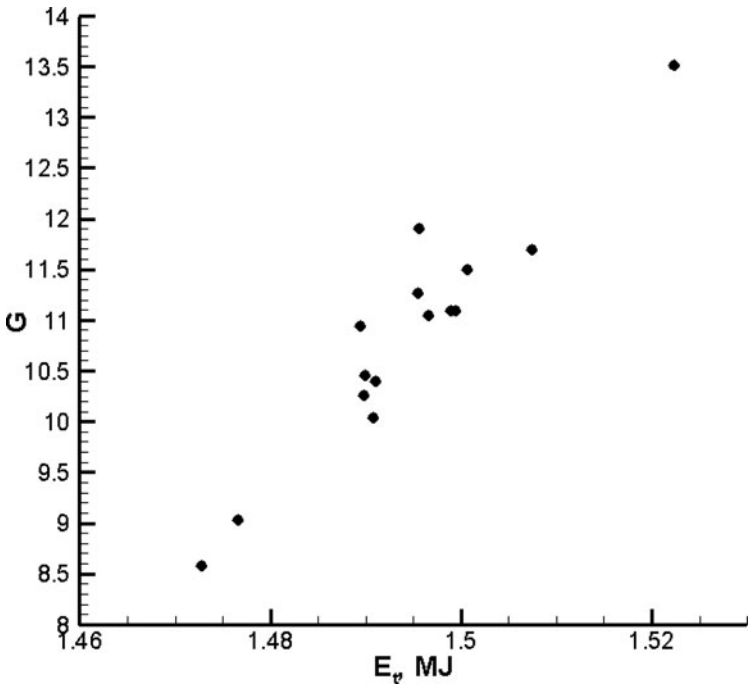

Fig. 7. Distribution of the thermonuclear gain *G* of conducted 1D calculations depending on the absorbed laser energy E_t.

https://doi.org/10.1017/S0263034615000671 Published online by Cambridge University Press

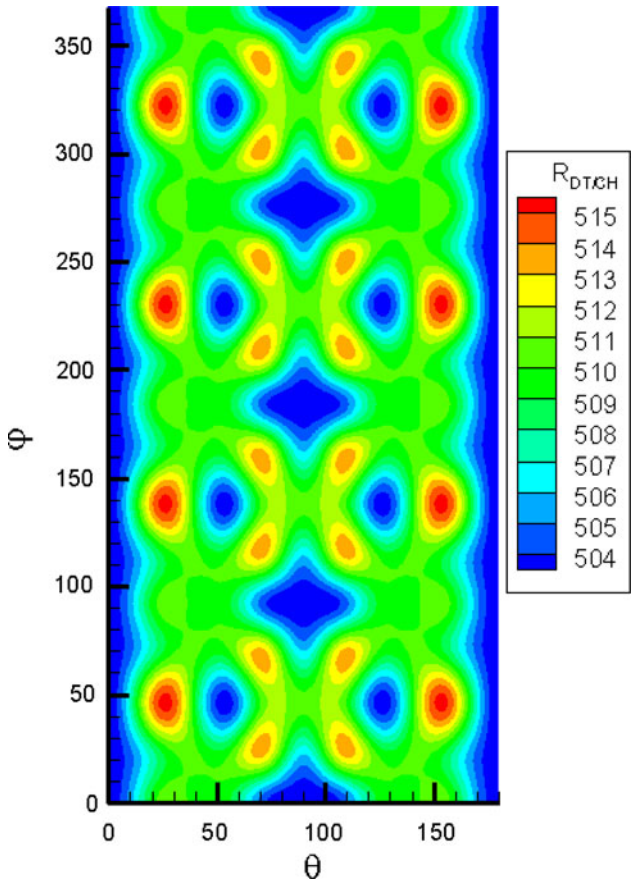

Fig. 8. Distribution of the radii of DT-ice outer surface at the time moment $t = 10$ ns.

at the nonlinear stage is significantly slower than at the linear one (Kuchugov *et al.*, 2012).

Thus it is evident that the development of instability in these irradiation conditions can lead to significant performance degradation of 1D compression. Further studies carried out using 2 and 3D hydrodynamic codes demonstrate influence extent of instabilities on the compression and burning of the target.

4. 2D SIMULATIONS

In the previous section we have shown that the results of the multi-dimensional (i.e., 2D and 3D) modeling will be substantially different from the 1D ones, showing close to the real dynamics of the compression and burning of thermonuclear target. The study of the processes in these cases gives a more complete and clear picture of the occurring physical phenomena. Note that in this case adequate description of the totality of the physical processes that may have not been implemented in (Edwards *et al.*, 2011, 2013; Clark *et al.*, 2013) plays a decisive role. As a possible illustration we present here the results of 2D calculations made by NUTCY program (Tishkin *et al.*, 1995; Lebo & Tishkin, 2006), which takes into account the necessary physics, that is, the local energy deposition from thermonuclear reactions, the electron heat conductivity and asymmetry of target irradiation as well.

Formation of the initial setting for the 2D calculations was performed according to the (Gus'kov *et al.*, 2010). Using the data obtained from 1D calculations, which correspond to the individual points on the sphere, we have approximated the data between these points to get 2D distribution. The procedure was performed for the profiles of three different angles $\varphi = 0.22$ and 46°, as well as for φ-averaged profiles. The calculated neutron yield N_Y and thermonuclear gain G are presented in Table 3. The table shows the degradation of the burning conditions in comparison with 1D spherically symmetrical simulations discussed in Section 3 of this paper. In particular, it should be noted that the observed gain G is approximately two times smaller than the one obtained in 1D calculations.

Figure 10 illustrates the density and temperature distributions at the time moment close to the target collapse for #1 and 3 calculations in Table 3 which received the highest and lowest values of the gain coefficient, respectively. A comparison of these two variants gives the following result. In case #3 the temperature drop in the central area is observed because of intense development of instabilities and mixing (as a consequence of more inhomogeneous irradiation), and this results in the decrease of the rate $\langle \sigma v \rangle_{DT}$ of the main thermonuclear reaction (Kozlov, 1962; Dolgoleva & Zabrodina, 2014). So, a slight inhomogeneity of irradiation leads to a significant decrease in the gain coefficient. However, the proposed target design remains to be applicable, that is, it is ignited.

5. A STEP TO FULL 3D PROCESS DESCRIPTION

3D simulations are one more step to a deeper understanding of the real process of thermonuclear target implosion. Mathematical modeling in this case presents an individual applied problem and is rather resource-intensive. In this paper we would like to give an example of a carried out 3D hydrodynamic calculation of target compression without heat conductivity and thermonuclear burning taken into account which, however, is indicative of the need to account of 3D effects.

Just as it was earlier (Gus'kov *et al.*, 2010), we take as the initial data for 3D simulation the distributions from the 1D calculation at the time moment corresponding to the time when the target shell deceleration starts. For the discussed target this moment precedes the target collapse by 1 ns, and defines the end of the laser pulse. A possibility of spherical target compression modeling with the help of the Euler code NUT-GPU (Kuchugov, 2014; Kuchugov *et al.*, 2014) in Cartesian coordinates was discussed in (Rozanov *et al.*, 2014). To demonstrate the experimentally realized surface shape, let us consider the model perturbation of DT-shell radial velocity. The perturbation amplitude constitutes 4% of 1D calculation value, that is,

https://doi.org/10.1017/S0263034615000671 Published online by Cambridge University Press

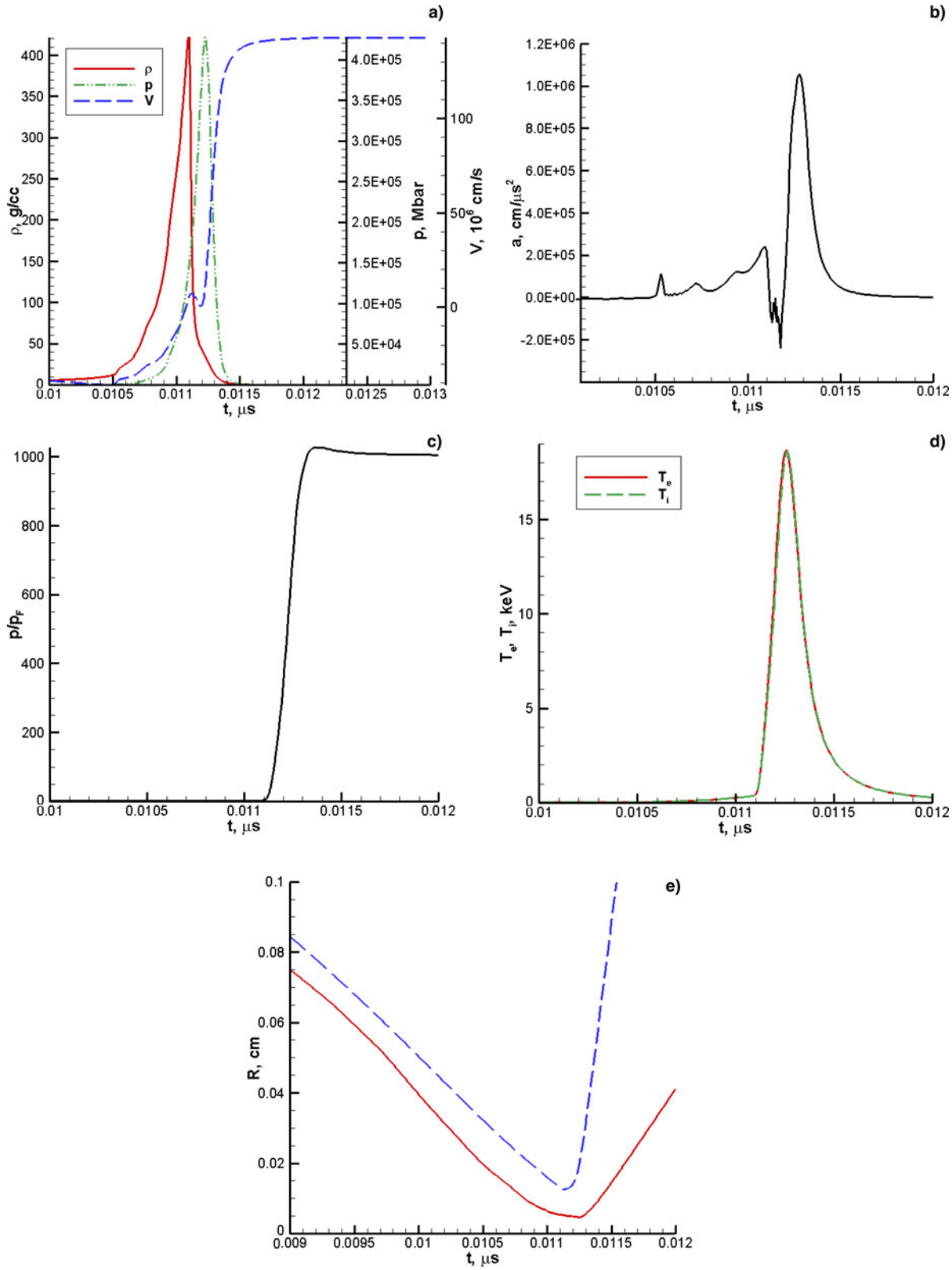

Fig. 9. Time dependencies (a) pressure, density, and radial velocity, (b) acceleration, (c) the parameter $\alpha = p/p_F$, (d) ion and electron temperature, (e) *R-t* diagram of inner and outer boundary of the DT-layer.

https://doi.org/10.1017/S0263034615000671 Published online by Cambridge University Press

Table 3. *Neutron yield and thermonuclear gain for the series of 2D calculations in comparison with 1D ones*

#	φ	## from Table 2	N_Y, 10^{18}	G
1	0°	1–6	5.4	5.85
2	22°	7–12	3.1	3.36
3	46°	13–18	2.6	2.82
4	φ-avareged profiles		4.6	4.98
5	1D calculations		7.9–12	8.58–13.5

$U_r^{3D} = U_r^{1D}\left[1 + 0.04Y_8^6(\theta, \phi)\right]$, where $Y_l^m(\theta, \phi)$ is a spherical harmonic. The simulation area is a cube with a side 0.9 cm, and the target is placed in its center. The cube side contains 640 cells of a computational grid.

In Figure 11 the density isolines with markers (left column) which correspond to DT-gas/DT-ice and DT-ice/ablator (CH) interfaces, and the isolines of radial velocity (right column) at the time moment $t = 11.1$ ns close to the target collapse are shown. The presented pictures demonstrate a typical Rayleigh–Taylor instability flow. The bubbles of a less dense matter are formed, and they penetrate through a denser matter which is still moving to the center. In the bubble tips the closest convergence of the inner and outer surface of DT-shell is observed, and there is a tendency to its destruction.

Note again that in the problem of thermonuclear fusion ignition it is absolutely essential that high velocity of the matter (or its part), that is, the kinetic energy, acquired due to external influence should be effectively converted into the internal one. This requires a fairly high degree of spherical symmetry of motion at all stages of implosion. As soon as the symmetry is violated, the conditions of energy conversion are becoming much worse. This is clearly seen in 2D problem (see Section 4) and, especially, in 3D one. The given example of 3D simulation confirms this statement, and shows complicated flow due to simple initial perturbations and at the same time the general symmetry of motion remains quite good. One can easily imagine the situation when not two counter-propagating jets

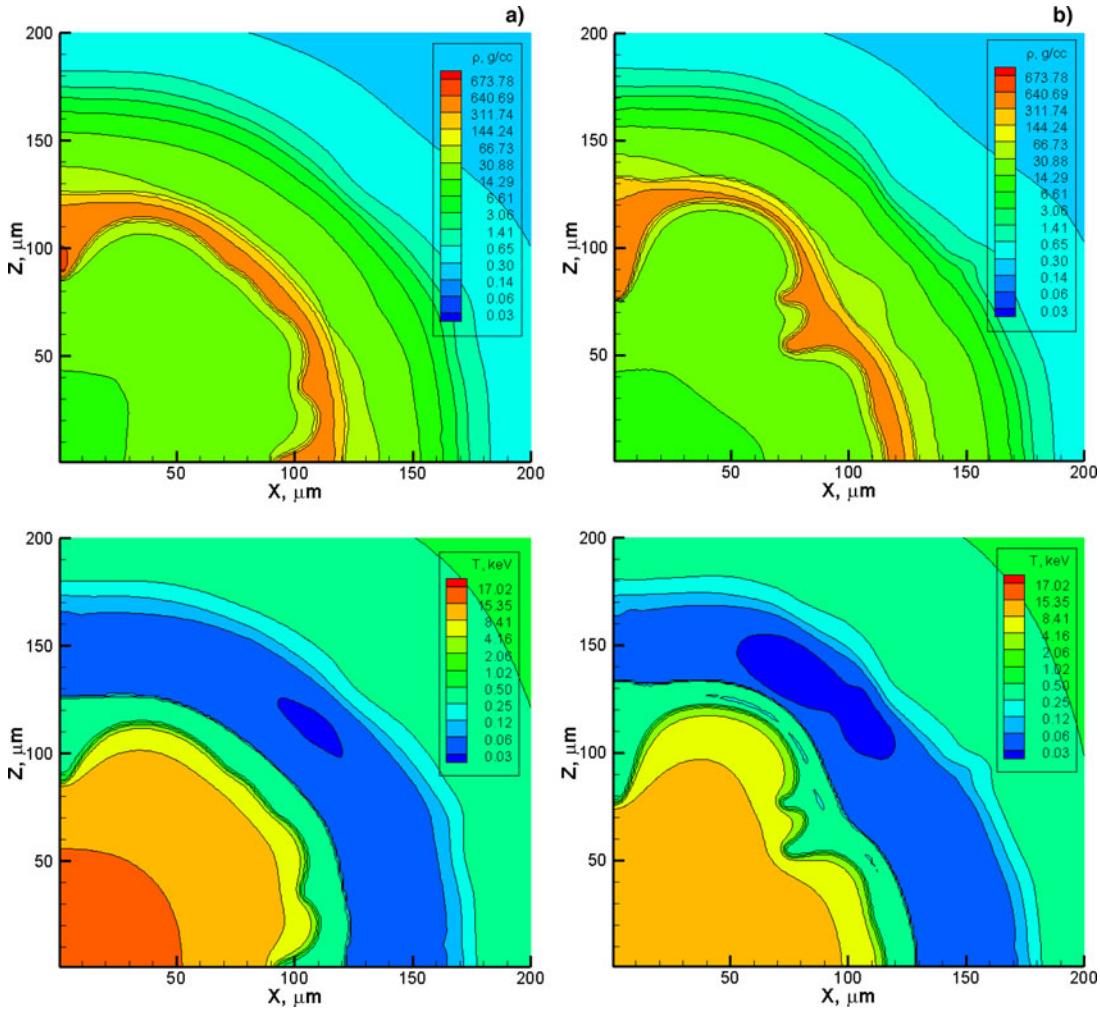

Fig. 10. Density and temperature distributions obtained in #1 (a) and #3 (b) calculations from Table 3 at the time moment $t = 11.1$ ns close to the target collapse.

https://doi.org/10.1017/S0263034615000671 Published online by Cambridge University Press

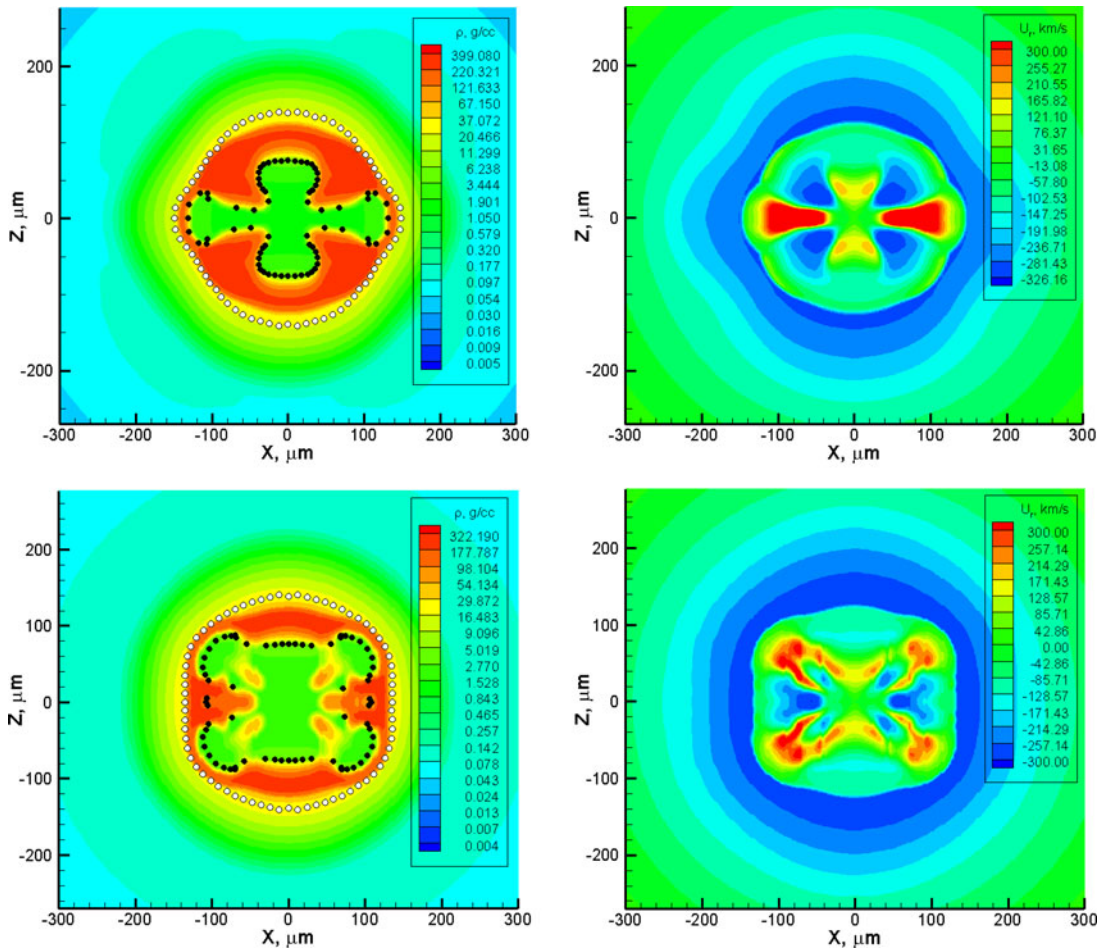

Fig. 11. Density and radial velocity isolines in plane cross-sections $y = x\mathrm{tg}(\varphi)$, $\varphi = 0°$ (the upper line) и $\varphi = 40°$ (the bottom line) at the time moment $t = 11.1$ ns. Black and white points correspond to the inner and outer boundaries of DT-layer.

(i.e., high-density areas) will collide, but the jets and the areas between the jets, and this will far more worsen the conditions of kinetic energy conversion into the potential one. Similar ideas have been put forward in a recent paper (Taylor & Chittenden, 2014), and the nature of such situations has been explained by the mode interaction in the real multimode initial perturbations. In future we are planning such 3D simulations in order to define quantitative parameters of thermonuclear target compression.

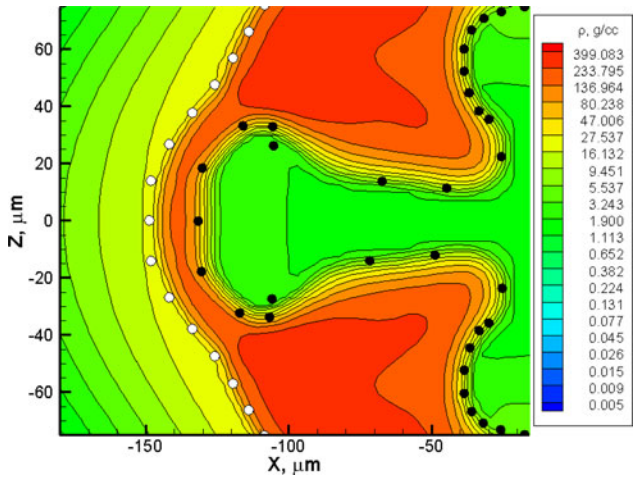

Fig. 12. Scale of convergence of inner and outer surface of the DT-ice layer in the bubble tips.

6. CONCLUSIONS

In conclusion we would like to note the following important results. The performed 1D simulations allow one to state that the symmetry of irradiation and compression of the targets of discussed design is quite acceptable to reach the needed gain. However, in experiments the conditions may be less favorable due to possible additional development of instabilities, and 2D and 3D simulations are indicative of this fact. It is important that in 3D simulations the degree of symmetry is decreased, and near the center of hot DT-gas the DT-ice jets have a small possibility of collision and deceleration, and, as a consequence, smaller efficiency of kinetic energy conversion into the potential one.

https://doi.org/10.1017/S0263034615000671 Published online by Cambridge University Press

ACKNOWLEDGMENTS

This work was partially supported by the Russian Foundation for Basic Research under grants No. 14-02-00270-a, and No. 14-01-00828-a.

REFERENCES

Afanas'ev, Yu.V., Gamalii, E.G., Demchenko, N.N. & Rozanov, V.B. (1982). The absorption of the laser radiation by the spherical target, taking into account refraction and hydrodynamics. *M.:Nauka, Trudy Fizicheskogo Instituta im. P.N. Lebedeva* **134**, 32–41.

Basov, N.G., Volosevich, P.P., Gamalii, E.G., Zakharenkov, Yu.A., Kiselev, A.E., Kurdyumov, S.P., Levanov, E.I., Rozanov, V.B., Rupasov, A.A., Samarskii, A.A., Sklizkov, G.V., Sotskii, E.N. & Shikanov, A.S. (1988). *The Thermal Conductivity of the Laser Crown Created by Laser*. Preprint No. 188. Moscow, Russia: Lebedev Physical Institute.

Besnard, D. (2008). Fusion with the Megajoule laser. *J. Phys. Conf. Ser*. **112**, 012004.

Boehly, T.R., Brown, D.L., Craxton, R.S., Keck, R.L., Knauer, J.P., Kelly, J.H., Kessler, T.J., Kumpan, S.A., Bucks, S.J., Letzring, S.A., Marshall, F.J., McCrory, R.L., Morse, S.F.B., Seka, W., Sowes, J.M. & Verdon, C.P. (1997). Initial performance results of the OMEGA laser system. *Opt. Commun*. **133**, 495–506.

Brandon, V., Canaud, B., Primout, M., Laffite, S. & Temporal, M. (2013). Marginally igniting direct-drive target designs for the laser megajoule. *Laser Part. Beams* **31**, 141–148.

Brandon, V., Canaud, B., Temporal, M. & Ramis, R. (2014). Low initial aspect-ratio direct-drive target designs for shock- and self-ignition in the context of the laser Megajoule. *Nucl. Fusion* **54**, 083016.

Clark, D.S., Hinkel, D.E., Eder, D.C., Jones, O.S., Haan, S.W., Hammel, B.A., Marinak, M.M., Milovich, J.L., Robey, H.F., Suter, L.J. & Town, R.P.J. (2013). Detailed implosion modeling of deuterium-tritium layered experiments on the National Ignition Facility. *Phys. Plasmas* **20**, 056318.

Dolan, T.J. (1981). *Fusion Research. Principles, Experiments and Technology*. New York: Pergamon Press.

Dolgoleva, G.V. (2013). *Numerical Solvation of Equations, Describing the Transfer of Heat by Electrons and Ions*. Preprint No. 71. Moscoe, Russia: Keldysh Institute of Applied Mathematics.

Dolgoleva, G.V. & Zabrodina, E.A. (2014). *Comparison of Two Models of Calculation of Thermonuclear Kinetics*. Preprint No. 68. Moscow, Russia: Keldysh Institute of Applied Mathematics.

Ebrardt, J. & Chaput, J.M. (2008). LMJ Project status. *J. Phys. Conf. Ser*. **112**, 032005.

Edwards, M.J., Lindl, J.D., Spears, B.K., Weber, S.V., Atherton, L.J., Bleuel, D.L., Bradley, D.K., Callahan, D.A., Cerjan, C.J., Clark, D., Collins, G.W., Fair, J.E., Fortner, R.J., Glenzer, S.H., Haan, S.W., Hammel, B.A., Hamza, A.V., Hatchett, S.P., Izumi, N., Jacoby, B., Jones, O.S., Koch, J.A., Kozioziemski, B.J., Landen, O.L., Lerche, R., MacGowan, B.J., MacKinnon, A.J., Mapoles, E.R., Marinak, M.M., Moran, M., Moses, E.I., Munro, D.H., Schneider, D.H., Sepke, S.M., Shaughnessy, D.A., Springer, P.T., Tommasini, R., Bernstein, L., Stoeffl, W., Betti, R., Boehly, T.R., Sangster, T.C., Glebov, V.Yu., McKenty, P.W., Regan, S.P., Edgell, D.H., Knauer, J.P., Stoeckl, C., Harding, D.R., Batha, S., Grim, G., Herrmann, H.W., Kyrala, G., Wilke, M., Wilson, D.C., Frenje, J., Petrasso, R., Moreno, K., Huang, H., Chen, K.C., Giraldez, E., Kilkenny, J.D., Mauldin, M., Hein, N., Hoppe, M., Nikroo, A. & Leeper, R.J. (2011). The experimental plan for cryogenic layered target implosions on the National Ignition Facility – The inertial confinement approach to fusion. *Phys. Plasmas* **18**, 051003.

Edwards, M.J., Patel, P.K., Lindl, J.D., Atherton, L.J., Glenzer, S.H., Haan, S.W., Kilkenny, J.D., Landen, O.L., Moses, E.I., Nikroo, A., Petrasso, R., Sangster, T.C., Springer, P.T., Batha, S., Benedetti, R., Bernstein, L., Betti, R., Bleuel, D.L., Boehly, T.R., Bradley, D.K., Caggiano, J.A., Callahan, D.A., Celliers, P.M., Cerjan, C.J., Chen, K.C., Clark, D.S., Collins, G.W., Dewald, E.L., Divol, L., Dixit, S., Doeppner, T., Edgell, D.H., Fair, J.E., Farrell, M., Fortner, R.J., Frenje, J., Gatu Johnson, M.G., Giraldez, E., Glebov, V.Yu., Grim, G., Hammel, B.A., Hamza, A.V., Harding, D.R., Hatchett, S.P., Hein, N., Herrmann, H.W., Hicks, D., Hinkel, D.E., Hoppe, M., Hsing, W.W., Izumi, N., Jacoby, B., Jones, O.S., Kalantar, D., Kauffman, R., Kline, J.L., Knauer, J.P., Koch, J.A., Kozioziemski, B.J., Kyrala, G., LaFortune, K.N., Le Pape, S., Leeper, R.J., Lerche, R., Ma, T., MacGowan, B.J., MacKinnon, A.J., Macphee, A., Mapoles, E.R., Marinak, M.M., Mauldin, M., McKenty, P.W., Meezan, M., Michel, P.A., Milovich, J., Moody, J.D., Moran, M., Munro, D.H., Olson, C.L., Opachich, K., Pak, A.E., Parham, T., Park, H.-S., Ralph, J.E., Regan, S.P., Remington, B., Rinderknecht, H., Robey, H.F., Rosen, M., Ross, S., Salmonson, J.D., Sater, J., Schneider, D.H., Seguin, F.H., Sepke, S.M., Shaughnessy, D.A., Smalyuk, V.A., Spears, B.K., Stoeckl, C., Stoeffl, W., Suter, L., Thomas, C.A., Tommasini, R., Town, R.P., Weber, S.V., Wegner, P.J., Widman, K., Wilke, M., Wilson, D.C., Yeamans, C.B. & Zylstra, A. (2013). Progress towards ignition on the National Ignition Facility. *Phys. Plasmas* **20**, 07050.

Garanin, S.G., Bel'kov, S.A. & Bondarenko, S.V. (2012). Concept of construction a laser system UFL-2M. *Book of Abstracts of Zvenigorod Int. Conf. on Plasma Physics and Controlled Fusion*, 6–10 February, Zvenigorod, Russia, p. 17.

Gus'kov, S.Yu., Demchenko, N.N., Zhidkov, N.V., Zmitrenko, N.V., Litvin, D.N., Rozanov, V.B., Stepanov, R.V., Suslov, N.A. & Yakhin, R.A. (2010). Analysis of direct-drive capsule compression experiments on the Iskra-5 laser facility. *J. Exp. Theor. Phys*. **111**, 466–483.

Kalitkin, N.N. (1978). *Numerical Methods*. Moscow: Nauka, p. 512.

Kozlov, B.N. (1962). The rates of thermonuclear reactions. *Atomnaya Energiya* **12**, 238.

Kuchugov, P., Zmitrenko, N., Rozanov, V., Yanilkin, Yu., Sin'kova, O., Statsenko, V. & Chernyshova, O. (2012). The evolution model of the Rayleigh-Taylor instability deveopmnent. *J. Rus. Las. Res*. **33**, 517–530.

Kuchugov, P.A. (2014). *Dynamics of turbulent mixing processes in laser targets*. PhD Thesis. Moscow, Russia: Keldysh Institute of Applied Mathematics.

Kuchugov, P.A., Shuvalov, N.D. & Kazenov, A.M. (2014). Simulation of the Gravitational Mixing on GPU. *Bull. Peoples' Friendship University of Russia, series Math., Inform., Phys*. **2**, 225–229.

Landen, O.L. (2014). NIF laser-matter experiments: Status and prospects. *Book of Abstracts of the 33rd European Conf. on*

Laser Interaction with Matter, 31 August–5 September 2014, Paris, France, p. 29.

Lebo, I.G. & Tishkin, V.F. (2006). *The Study of Hydrodynamic Instability in Problems of Laser Fusion by Methods of Mathematical Modeling*. Moscow: FIZMATLIT, p. 304.

Lindl, J. (1995). Development of the indirect-drive approach to inertial confinement fusion and the target physics basis for ignition and gain. *Phys. Plasmas* **2**, 3933.

Miller, G.H., Moses, E.I. & Wuest, C.R. (2004). The National Ignition Facility. *Opt. Eng*. **43**, 2841–2853.

Miquel, J.L. (2014). The laser Megajoule facility: Current status and program overview. *Book of Abstracts of the 33rd European Conf. on Laser Interaction with Matter*, August 31–September 5 2014, Paris, France, p. 25.

Moses, E.I., Boyd, R.N., Remington, B.A., Keane, C.J. & Al-Ayat, R. (2009). The National Ignition Facility: Ushering in a new age for high energy density science. *Phys. Plasmas* **16**, 041006.

Rozanov, V.B., Gus'kov, S.Yu., Vergunova, G.A., Demchenko, N.N., Stepanov, R.V., Doskoch, I.Ya., Yakhin, R.A., Bel'kov, S.A., Bondarenko, S.V. & Zmitrenko, N.V. (2013). Direct Drive Targets for the Megajoule Installation UFL-2M. *Book of Abstracts of the Int. Conf. of Inertial Fusion and Application Science*, 8–13 September 2013, Nara, Japan, p. 236.

Rozanov, V.B., Gus'kov, S.Yu., Vergunova, G.A., Demchenko, N.N., Stepanov, R.V., Doskoch, I.Ya., Yakhin, R.A. & Zmitrenko, N.V. (2015). Direct Drive targets for the megajoule facility UFL-2M. *J. Phys. Conf. Ser.* **651**, 012017.

Rozanov, V.B., Zmitrenko, N.V., Kuchugov, P.A., Stepanov, R.V., Statsenko, V.P., Yanilkin, Yu.V. & Yakhin, R.A. (2014). Hydrodynamic instabilities and mixing in the direct-drive laser targets for the megajoule scale facilities. *Book od Abstracts of the 33rd European Conf. on Laser Interaction with Matter*, 31 August–5 September 2014, p. 101.

Taylor, S. & Chittenden, J.P. (2014). Effects of perturbations and radial profiles on ignition of inertial confinement fusion hotspots. *Phys. Plasmas* **21**, 062701.

Tishkin, V.F., Nikishin, V.V., Popov, I.V. & Favorskii, A.P. (1995). Finite difference schemes of three-dimensional gas dynamics for the study of Richtmyer–Meshkov instability. *Matem. Mod*. **7**, 15–25.

Volosevich, P.P., Gus'kov, S.Yu., Levanov, E.I., Rozanov, V.B. & Sirotenko, N.G. (1995). *Mathematical Modeling of Laser Compression and Burning of Two-stage Thermonuclear Targets*. Preprint No. 18. Moscow, Russia: Institute of Mathematical Modelling.

Volosevich, P.P., Kosyrev, V.I. & Levanov, E.I. (1978). *On Account of the Restriction of Heat Flux in the Numerical Experiment*. Preprint No. 21. Moscow, Russia: Institute of Applied Mathematics.

Zmitrenko, N.V., Karpov, V.Ya., Fadeev, A.P., Shelaputin, I.I. & Shpatakovskaya, G.V. (1983). Description of the physical processes in the DIANA program for calculations of problems of laser fusion. *Voprosy Atomnoy Nauki i Tekhniki* (*VANT*) *Series Methods and Software for Numerical Solution of Problems of Mathematical Physics* **2**, 34–37.

https://doi.org/10.1017/S0263034615000671 Published online by Cambridge University Press